# PHOTOABSORPTION CONVECTION IN CAVITIES

B. M. Berkovskii and E. F. Nogotov

UDC 536.25:538.345

An economical finite-difference system is given for solving problems in convection caused by absorption of radiation. Threshold effects are predicted and examined in detail.

The passage of an electromagnetic wave through a material is accompanied by absorption, i.e., irreversible conversion of part of the radiation to heat, which alters the temperature distribution in the material. A heavy fluid shows thermal convection due to gravitational forces, and any change in temperature distribution due to the radiation also alters the structure of the convection. Convective heat transfer in turn tends to correct the temperature and other distributions. The convective phenomena react back on the electromagnetic waves via the dependence of the dielectric constant and magnetic susceptibility on the thermodynamic characteristics; one gets a complex pattern of interaction between the electromagnetic, thermal, and dynamic fields.

Consider the structure and rate of the steady-state convection caused in a heavy fluid by absorption of electromagnetic waves in the visible frequency range. We assume that the boundaries of the region where the convection occurs are kept at a constant temperature or are thermally insulated and immobile. We call the convection excited by light under such conditions photoabsorption convection PAC.

1. The problem can be formulated mathematically, because the propagation of electromagnetic waves in a material is described by Maxwell's equations [1, 2]. In the optical frequency range, if the absorption is not too strong, one can use instead of the very complex Maxwell's equations the simple ray or geometrical optics, which is a good approximation [3-6]. We give the following form to the basic equations for the ray approximation. The equation for a ray path $\mathbf{r} = \mathbf{r}(s)$ is [4, 5]

$$\frac{d}{ds}\left(n\frac{d\mathbf{r}}{ds}\right) = \nabla n, \tag{1}$$

where n is the refractive index; $\mathbf{r}$ is the radius vector of a point on the path; and ds is an element along the path. The intensity change dI(s) along the path is governed by two factors: the change in a cross section of the beam and absorption [4]:

$$dI(s) = I(s)\frac{dn - \nabla^2 L ds}{n} + kI(s)\,ds, \tag{2}$$

$$L = \int_0^s n ds, \tag{3}$$

where k is absorption coefficient and L is the eiconal.

The following is the amount of radiation energy converted to heat:

$$Q(s) = kI(s) = kI_0(n/n_0)\exp\left\{-\int_0^s [(\nabla^2 L/n) + k]\,dz\right\}. \tag{4}$$

Convected heat transfer is described by equations representing the conservation of energy with allowance for the sources of (4), together with equations for the conservation of mass and momentum [7]. These are put not in general form but for the following particular case.

Institute of Heat and Mass Transfer, Academy of Sciences of the Belorussian SSSR, Minsk. Translated from Inzhenerno-Fizicheskii Zhurnal, Vol. 19, No. 6, pp. 1012-1020, December, 1970. Original article submitted June 4, 1970.

Consider the two-dimensional PAC in the horizontal cavity of square cross section. The light beam is perpendicular to the surface and uniformly illuminates the upper wall of the cavity $x(y, x_0, x_0')$, $x_0' = 0$. The walls are considered solid and transparent, while the liquid in the cavity is an absorbing one. The thermal boundary conditions at the walls are assumed to be of two types: 1) all the walls are isothermal; 2) the horizontal boundaries have constant and identical temperatures, while the side walls are thermally insulated.

The dimensionless equations take the form:

$$\frac{d^2x}{dy^2} = \left[\frac{\partial n_*}{\partial x} - x'\frac{\partial n_*}{\partial y}\right]\frac{1+x'^2}{n_*}, \tag{5}$$

$$L_* = n_* + \int_1^y n_* \sqrt{1+x'^2}\, dy, \tag{6}$$

$$Q^* = Bk_* \,\mathrm{Hk}\, n_* \exp\left[-\int_1^y \sqrt{1+x'^2}\left(\frac{\nabla^2 L_*}{n_*} + Bk_*\right) dy\right], \tag{7}$$

$$k = k_0 k_*,\ k_* = 1 + \mathrm{Hn}\,\Theta,\ B = ak_0,\ \mathrm{Hn} = \zeta T_*,$$
$$\mathrm{Hk} = a^4 \beta g I_0/(\nu^3 \rho c),\ L = L_* a n_0,\ n = n_0 n_*, \tag{8}$$
$$n_* = 1 + \mathrm{Hp}\Theta,\ \Theta = (T - T_0)/T_*,$$

$$\frac{\partial \Theta}{\partial t} = \frac{1}{p}\nabla^2\Theta + \frac{\partial}{\partial y}\left(\Theta\frac{\partial \psi}{\partial x}\right) - \frac{\partial}{\partial x}\left(\Theta\frac{\partial \psi}{\partial y}\right) + Q, \tag{9}$$

$$\frac{\partial \omega}{\partial t} = \nabla^2\omega + \frac{\partial}{\partial y}\left(\omega\frac{\partial \psi}{\partial x}\right) - \frac{\partial}{\partial x}\left(\omega\frac{\partial \psi}{\partial y}\right) + \frac{\partial \Theta}{\partial x}, \tag{10}$$

$$\nabla^2\psi = -\omega. \tag{11}$$

We take as units of distances x and y, time t, current function $\psi$, and temperature $\Theta$ the length of the side of a square $a$, the ratio $a^2/\nu$, the kinematic viscosity $\nu$, and the quantity $T_* = \nu^2/g\beta a^3$, respectively; P is the Prandtl number; B is the optical depth; and Hk, Hp, and Hm are parameters characterizing the intensity of the radiation energy, and the dependence of the absorption and refraction coefficients on temperature. The following are the boundary conditions for the current function and temperature at the boundaries $\Gamma$:

$$u(\Gamma) = v(\Gamma) = 0, \qquad \text{a) } \Theta(\Gamma) = 0, \tag{12}$$

$$\text{b) } \Theta_x(0, y) = \Theta_x(1, y) = 0,\ \Theta(x, 0) = \Theta(x, 1) = 0. \tag{13}$$

A study has already been reported [9] for PAC without allowance for the reaction of the convection on the light propagation; this indicated the possibility that there are threshold effects, one of which is here studied in detail.

There is particular interest in the PAC for thermally-insulated vertical boundaries; system (5)-(13) for this case permits a solution corresponding to nonisothermal mechanically equilibrium state $x = x_0$, $\psi = 0$, $\omega = 0$, $\Theta = \Theta(y)$. If the absorption coefficient is independent of temperature, the temperature distribution takes the form

$$\Theta = B\,\mathrm{Hk}\exp(-B)\,[1 + y(\exp B - 1) - \exp(By)]. \tag{14}$$

The temperature distribution of (14) shows that the maximum temperature is attained within the cavity, which means that this mechanically equilibrium state may be unstable; in fact, in the upper part of the cavity the temperature distribution corresponds to the well-known mechanically unstable state with heating from below. Convection can arise in this part of the cavity if the negative temperature gradient is sufficiently large. Large temperature gradients are obtained as the incident intensity is raised, so for otherwise constant conditions one expects instability to arise as parameter Hk is increased.

2. System (5)-(13) has been solved numerically by a method of grids; the steady-state solution was obtained by establishing all the characteristics of the motion for $t \to \infty$. An approximation to the solution was derived with a finite number of points in the grid, which had coordinates $x_i = i\Delta x$, $y_j = j\Delta y$ and with a digitized time $t_n = n\tau$, where i, j, and n are integers. The grid was chosen square so that the grid parameters in the x and y directions were equal, i.e., $\Delta x = \Delta y = h$.

To obtain a numerical solution one first uses a finite-difference scheme of variables for the directions of the predictor–corrector type, in which the second derivatives were replaced by the ordinary central differences, while the first derivatives with respect to space were approximated by directional differences with distinct directions; however, the calculations showed that the machine time required would be very substantial before the steady-state solution was obtained on account of frequent resort to external stores.

We then developed a finite-difference scheme that incorporates the advantages of integral-interpolation (balance) schemes [11] and schemes that use directional derivatives [10, 12]. The basic features of the scheme may be illustrated by reference to Eq. (9).

Consider the region around some internal node in the net $(x_i, y_j)$; we integrate (9) over the reference volume $D(x_{i-\frac{1}{2}} \le x \le x_{i+\frac{1}{2}}, y_{j-\frac{1}{2}} \le y \le y_{j+\frac{1}{2}})$, with the time derivative assumed constant within D and equal to $(\partial\Theta/\partial t)_{i,j}$.

The second spatial derivatives were replaced by central differences, which gave

$$h^2\left(\frac{\partial\Theta}{\partial t}\right)_{i,j} = \frac{1}{P}(\Theta_{i+1,j} + \Theta_{i-1,j} + \Theta_{i,j+1} + \Theta_{i,j-1} - 4\Theta_{i,j}) - h^2Q$$
$$-\Theta_{i+\alpha,j}(\psi_{i+\frac{1}{2},j+\frac{1}{2}} - \psi_{i+\frac{1}{2},j-\frac{1}{2}}) + \Theta_{i-\beta,j}(\psi_{i-\frac{1}{2},j+\frac{1}{2}} - \psi_{i-\frac{1}{2},j-\frac{1}{2}})$$
$$+\Theta_{i,j+\gamma}(\psi_{i+\frac{1}{2},j+\frac{1}{2}} - \psi_{i-\frac{1}{2},j+\frac{1}{2}}) - \Theta_{i,j-\eta}(\psi_{i+\frac{1}{2},j-\frac{1}{2}} - \psi_{i-\frac{1}{2},j-\frac{1}{2}}),$$

where $\alpha$, $\beta$, $\gamma$, and $\eta$ can take the values of either 0 or 1. The choice of value is dependent on the sign of the velocity between the corresponding points in the grid ($v_x = \partial\psi/\partial y$, $v_y = -\partial\psi/\partial x$). If the velocity is positive, then one takes the left (lower) node; if the velocity is negative, then one takes the right (upper) node. This order of taking the nodes meets more exactly the difference laws for conservation, which corresponds to improved divergence in the scheme. We replace the values of $\psi$ in the fractional nodes by a quarter of the sum of the values of $\psi$ in the adjacent integral nodes, which gives

$$h^2\left(\frac{\partial\Theta}{\partial t}\right)_{i,j} = \left(A_{i+1,j} + \frac{1}{P}\right)\Theta_{i+1,j} + \left(A_{i-1,j} + \frac{1}{P}\right)\Theta_{i-1,j}$$
$$+\left(A_{i,j+1} + \frac{1}{P}\right)\Theta_{i,j+1} + \left(A_{i,j-1} + \frac{1}{P}\right)\Theta_{i,j-1} - \frac{4}{P}\Theta_{i,j} - (A_{i+1,j} + A_{i-1,j} + A_{i,j+1} + A_{i,j-1})\Theta_{i,j} + h^2Q,$$
$$A_{i+1,j} = [(\psi_{i+1,j-1} + \psi_{i,j-1} - \psi_{i,j+1} - \psi_{i+1,j+1}) + |\psi_{i+1,j-1} + \psi_{i,j-1} - \psi_{i,j+1} - \psi_{i+1,j+1}|]/8,$$
$$A_{i-1,j} = [(\psi_{i-1,j+1} + \psi_{i,j+1} - \psi_{i,j-1} - \psi_{i-1,j-1}) + |\psi_{i-1,j+1} + \psi_{i,j+1} - \psi_{i,j-1} - \psi_{i-1,j-1}|]/8,$$
$$A_{i,j+1} = [(\psi_{i+1,j+1} + \psi_{i+1,j} - \psi_{i-1,j} - \psi_{i-1,j+1}) + |\psi_{i+1,j+1} + \psi_{i+1,j} - \psi_{i-1,j} - \psi_{i-1,j+1}|]/8,$$
$$A_{i,j-1} = [(\psi_{i-1,j-1} + \psi_{i-1,j} - \psi_{i+1,j} - \psi_{i+1,j-1}) + |\psi_{i-1,j-1} + \psi_{i-1,j} - \psi_{i+1,j} - \psi_{i+1,j-1}|]/8.$$

An analogous expression is obtained on integrating the equation for the circulation; the differences lie only in the coefficients where in place of $1/P$ we take unity, and also in the source.

We now integrate the two equations with respect to time with limits from $t_n$ to $t_{n+1}$. The coefficients and the sources here are assumed to be constant throughout a time step; the temperatures and the circulations at the nodes $(x_{i+1}, y_j)$ and $(x_i, y_{j+1})$ relate to time $t_n$, while those at $(x_{i-1}, y_j)$ and $(x_i, y_{j-1})$ relate to time $n+1$. As regards the node of $(x_i, y_j)$, we obtain sufficient accuracy in approximation to the initial equations for $\Theta$ and $\omega$ as regards the convective terms while taking them all at a point $t_{n+1}$, while the corresponding diffusion terms are taken as differences between the points $t_n$ and $t_{n+1}$. As a result, the equations for the temperature and circulation take the following finite-difference form:

$$\Theta^+_{i,j} = \left\{\left(A_{i+1,j} + \frac{1}{P}\right)\Theta_{i+1,j} + \left(A_{i-1,j} + \frac{1}{P}\right)\Theta^+_{i-1,j}\right.$$
$$\left.+\left(A_{i,j+1} + \frac{1}{P}\right)\Theta_{i,j+1} + \left(A_{i,j-1} + \frac{1}{P}\right)\Theta^+_{i,j-1} + \left(\frac{h^2}{\tau} - \frac{2}{P}\right)\Theta_{i,j} + h^2Q\right\}$$
$$\times\left\{\frac{h^2}{\tau} + \frac{2}{P} + A_{i+1,j} + A_{i-1,j} + A_{i,j+1} + A_{i,j-1}\right\}^{-1}, \qquad (15)$$

$$\omega^+_{i,j} = \Big\{(A_{i+1,j}+1)\,\omega_{i+1,j} + (A_{i-1,j}+1)\,\omega^+_{i-1,j} + (A_{i,j+1}+1)\,\omega_{i,j+1}$$
$$+ (A_{i,j-1}+1)\,\omega^+_{i,j-1} + \left(\frac{h^2}{\tau} - 2\right)\omega_{i,j} + \frac{h}{2}(\Theta^+_{i+1,j} - \Theta^+_{i-1,j})\Big\}\Big\{\frac{h^2}{\tau}$$
$$+ 2 + A_{i+1,j} + A_{i-1,j} + A_{i,j+1} + A_{i,j-1}\Big\}^{-1}. \tag{16}$$

Here for convenience in writing the formulas we have introduced the following symbols: + denotes that the value of a function is taken at time $t_{n+1}$, while the absence of this superscript indicates that the function is taken at $t_n$.

The boundary conditions for $\psi$ and for the temperature take the following form:

$$\psi_{i,0} = \psi_{i,J} = \psi_{0,j} = \psi_{J,j} = 0,$$
$$\text{a)}\ \Theta_{i,0} = \Theta_{i,J} = \Theta_{0,j} = \Theta_{J,j} = 0, \tag{17}$$

$$\text{b)}\ \Theta_{0,j} = \frac{1}{3}(4\Theta_{1,j} - \Theta_{2,j}),\quad \Theta_{J,j} = \frac{1}{3}(4\Theta_{J-1,j} - \Theta_{J-2,j}),\quad \Theta_{i,0} = \Theta_{i,J} = 0. \tag{18}$$

Unifortunately, it was impossible to obtain exact analytical expressions for the boundary values for the circulation; for $\omega$, the boundary conditions were obtained approximately by expanding $\psi(x, y, t)$ as a Taylor series near the boundary. For the lower boundary, for example, they take the form

$$\omega_{i,0} = -\frac{8\psi_{i,1} - \psi_{i,2}}{2h^2},$$

and the boundary conditions for the other boundaries are analogous.

System (5)-(8), (11), (15), (16) with conditions (17)-(19) was solved in the following sequence. We assume that we know the values of $\Theta$, $\omega$, and $\psi$ at instant $t_n$ for the whole region; the next time step begins with calculation of $n_*$ and $k_*$, followed by calculation of the path. For this purpose, the Runge–Kutta method is used to integrate (5), and at points $y_m = mh/2$ ($m = 1, 2, 3, \ldots, 2J$) one determines x and x' with a set accuracy. We find Q from (7). The definite integrals appearing in the exponents were calculated by Simpson's formula. Then linear extrapolation was used to extend the results for Q over the nodes. After this, (15) enabled one to calculate $\Theta^+$ over all internal points in the region. Then from (8) we found $\omega^+$. The new values for $\omega$ were then introduced into Eq. (11), which was solved by the method of upper relaxation [13]. Then from (19) we calculated the new boundary conditions for $\omega$.

In this way, we obtained the distribution of $\Theta$, $\omega$, and $\psi$ for time $t_{n+1}$, from which one can proceed to the next time step.

To save machine time, the values of the $Q_{i,j}$ were calculated at each time only as long as they altered by more than a set proportion (1%), and after this they were corrected only every 10 steps in time. As the initial approximation for $t = 0$ we usually assumed either $\Theta_{i,j} = \omega_{i,j} = \varphi_{i,j} = 0$ or the values of the quantities obtained for other values of the parameters Hk, B, or P. The calculations showed that the steady-state solution was not dependent on the form of the initial approximation or on the magnitude of $\tau$.

We examined the stability by Neumann's method [14], which showed that the above difference scheme is stable for $\tau \leq h^2/2$; it is readily shown that for $\tau \sim h^2$ it approximates the initial system of (9) and (10) with an order $o(h)$.

The rate of approach to the solution was considerably accelerated because in each time step from $t_n$ to $t_{n+1}$ we used at the points $(x_{i-1}, y_j)$, $(x_i, y_{j-1})$ and partly at $(x_i, y_j)$ the values of $\Theta^+$, $\omega^+$ already calculated for time $t_{n+1}$. This doubled the rate of solution, for example, by comparison with the method of [12]. Also, it considerably reduced the volume of machine store because the new values $\Theta^+$ and $\omega^+$ can at once be written in place of $\Theta$ and $\omega$, respectively, so the above finite-difference scheme can be useful for computers with small volumes of operative store.

All the calculations were carried out with an M-220 computer; the results discussed below were obtained with a 21 × 21 grid ($h = 0.05$). The time step was constant at $\tau = 0\ 001$, which provided good accuracy with reasonable consumption of machine time. The accuracy of the numerical scheme was checked

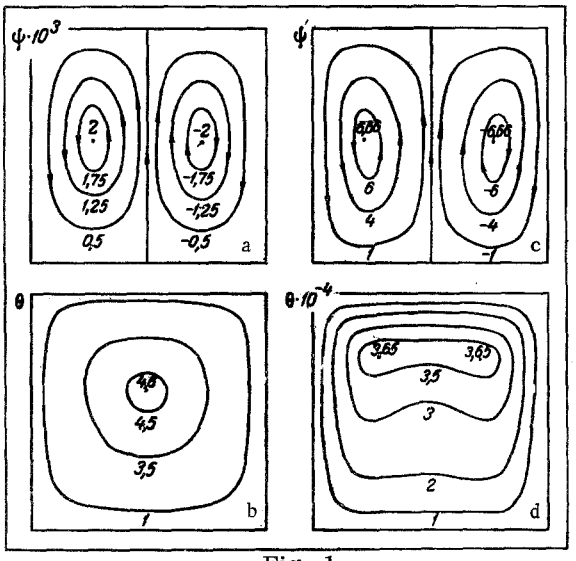


Fig. 1

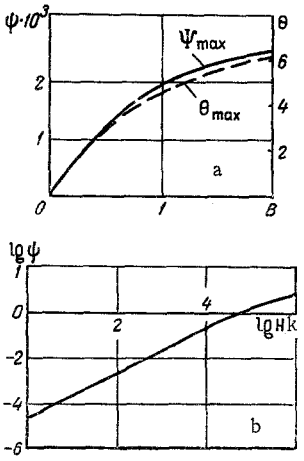


Fig. 2

Fig. 1. Structure of convection (a, c) and temperature profiles (b, d) for B = 1, Hk = $10^2$ (a, b); $10^6$ (c, d) with isothermal boundaries.

Fig. 2. $\psi_{max}$ (solid line) and $\Theta_{max}$ (dotted line) vs B for Hk = $10^2$ (a) and logarithmic dependence of $\psi_{max}$ on Hk for B = 1 (b).

by performing calculations for the case of thermally insulated side walls with Hk < Hk*; the solution agreed well with the analytical solution, which can be obtained for this case, the difference being less than 1%.

3. The calculations were performed with the following values of the parameters:

$$0 < P \leqslant 2;\ 0 < Hk \leqslant 10^6;\ 0 < B \leqslant 2;\ Hp = 0;\ Hn = 0; 10^{-6}.$$

The isothermal boundary conditions of (18a) cause a cellular convection to arise in the cavity; Fig. 1 shows the current lines (a, c) and the isotherms (b, d) for B = 1 with P = 1, Hn = 0, Hk = $10^2$ (a, b) and Hk = $10^6$ (c, d). Figure 1 shows that absorption of light entering from above gives rise to two oval cells rotating in opposite directions, which are symmetrically disposed relative to the vertical axis of the square and, as calculations show, they have forms that vary little with Hk and B. Only for Hk > $10^5$ do the centers of the squares move appreciably towards the vertical boundaries, and the cells themselves rise slightly at the same time.

The isotherms are closed lines approximating to circles; their shape varies little as B goes from 0 to 2. The position of $\Theta_{max}$ move upwards somewhat as B increases; the upward shift in the maximum temperature is observed also when Hk increases, and then for a sufficiently large Hk > $10^4$ one gets two centers, when the temperature attains maximal values (Fig. 1b).

Figure 2a shows how $\psi_{max}$ and $\Theta_{max}$ vary with B for Hk = $10^2$; these increase monotonically with B, and the rates of growth diminish appreciably. Figure 2b shows the dependence of $\log \psi_{max}$ on log Hk for B = 1; for Hk < $10^5$ the result is a straight line of slope 0.5, which corresponds to a relationship of the form $\psi_{max} \sim \sqrt{B}$.

In the threshold problem of (18b) we found critical values of Hk* for various values of B; Fig. 3a shows the dependence of $\psi_{max}$ on Hk for various B (I corresponds to B = 1; II to B = 1.5; and III to B = 0.5). Figure 3a shows that, up to a certain Hk*, $\psi_{max} = 0$, which means that there is no convection; further increase in Hk causes the convection to develop rapidly. The Hk* is very much dependent on B, as Fig. 3b shows; as B approaches 0, Hk* increases considerably, while increase in B causes Hk to decrease, and for B ~ 1.5 it attains its minimum, with further increase in B causing Hk* again to increase, but much more slowly than before.

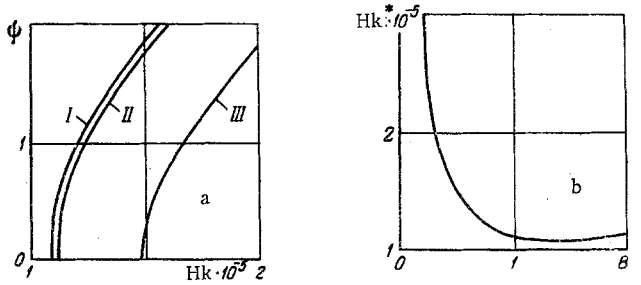


Fig. 3. $\psi_{max}$ vs Hk for B = 1 (I); 2) (II); 0.5 (III) (a) and Hk vs B (b).

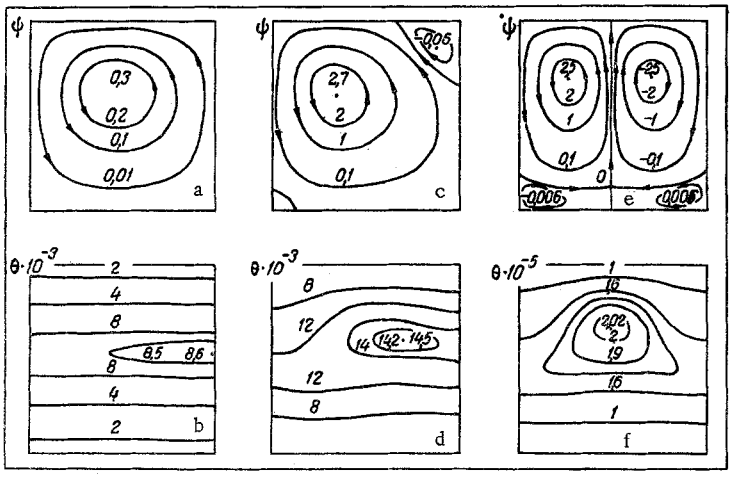


Fig. 4. Structure of convection and temperature profile at heat-insulated sides for Hk = $1.1 \cdot 10^5$ (a, b); $2 \cdot 10^5$ (c, d); $3 \cdot 10^5$ (e, f) (Hk* = $1.09 \cdot 10^5$; B = 1).

Figure 4 shows current lines (a, c, e) and isotherms (b, d, f) for B = 1 of Hk of: a and b) $1.1 \cdot 10^5$; c and d) $2 \cdot 10^5$; e and f) $3 \cdot 10^5$. The isotherms are straight lines parallel to the x axis in the absence of convection. There is a local rise in temperature at one of the boundaries when Hk is reached; as a rule, $\Theta_{max}$ is observed on the right boundary and corresponds to convected motion in the counterclockwise direction. There are also cases where $\Theta_{max}$ occurs at the left wall, and then the circulation is clockwise. The sense of the convection is governed by purely random factors. Hk > Hk* gives circular convection (Fig. 4a); the isotherms remain straight lines, except near the center (Fig. 4b). They become more curved as Hk increases and $\Theta_{max}$ shifts; a second cell with opposite motion arises.

Further increase in Hk shifts $\Theta_{max}$ to the center, and we get the convection of Fig 4e and f, which is stable for a fairly large range in Hk; only for Hk > $10^8$ does one get oscillations analogous to those of [15].

## LITERATURE CITED


1. L. D. Landau and E. M. Lifshits, Mechanics of Continuous Media [in Russian], GITTL (1954).
2. V. L. Ginzburg, Propagation of Electromagnetic Waves in a Plasma [in Russian], Nauka, GRFMI (1967).
3. F. A. Korolev, Theoretical Optics [in Russian], Vysshaya Shkola, Moscow (1966).
4. M. Born and E. Holt, Principles of Optics, Pergamon Press (1965).
5. Yu. A. Kravtsov, "Complex rays and complex acoustics," Izv. VUZ, Radiofizika, 10, Nos. 9-10 (1967).
6. Yu. S. Saysov, Paper at the Second All-Union Conference on Wave Diffraction [in Russian], Gor'kii (1962).
7. A. V. Lykov and Yu. A. Mikhailov, Theory of Heat and Mass Transfer [in Russian], Gosénergoizdat (1963).
8. B. M. Berkovskii, O. G. Martynenko, A. M. Zhilkin, and O. N. Porokhov, Thermohydrodynamic Light Guides [in Russian], Nauka i Tekhnika, Minsk (1969).

9. B. M. Berkovskii, in: Thermohydrodynamic Light Guides [in Russian], Nauka i Tekhnika, Minsk (1970), p. 78.
10. A. D. Cosman, W. M. Pun, A. K. Runchal, and D. B. Spalding, Heat and Mass Transfer in Recirculating Flows, Academic Press, London–New York (1969).
11. A. N. Tikhonov and A. A. Samarskii, The Equations of Mathematical Physics [in Russian], Nauka, Moscow (1966).
12. K. E. Torrance and J. A. Rockett, J. Fluid Mech., 36, Part 1, 33-54 (1969).
13. W. Bazoff and J. Foresight, Difference Methods of Solving Differential Equations in Partial Derivatives [Russian translation], IL (1963).
14. B. Eddy, Naval Ordnance Laboratory Memorandum, 10 (1949).